

# Soft Matter

Accepted Manuscript



This is an *Accepted Manuscript*, which has been through the Royal Society of Chemistry peer review process and has been accepted for publication.

*Accepted Manuscripts* are published online shortly after acceptance, before technical editing, formatting and proof reading. Using this free service, authors can make their results available to the community, in citable form, before we publish the edited article. We will replace this *Accepted Manuscript* with the edited and formatted *Advance Article* as soon as it is available.

You can find more information about *Accepted Manuscripts* in the [Information for Authors](#).

Please note that technical editing may introduce minor changes to the text and/or graphics, which may alter content. The journal's standard [Terms & Conditions](#) and the [Ethical guidelines](#) still apply. In no event shall the Royal Society of Chemistry be held responsible for any errors or omissions in this *Accepted Manuscript* or any consequences arising from the use of any information it contains.



Journal Name

ARTICLE

## Structure of lipid multilayers via drop casting of aqueous liposome dispersions

Beatrice Sironi,<sup>a</sup> Tim Snow,<sup>a</sup> Christian Redeker,<sup>a</sup> Anna Slastanova,<sup>a</sup> Oier Bikondoa,<sup>b,c</sup> Thomas Arnold,<sup>d</sup> Jacob Klein,<sup>e</sup> and Wuge H. Briscoe<sup>a†</sup>

Received 00th January 20xx,  
Accepted 00th January 20xx

DOI: 10.1039/x0xx00000x

www.rsc.org/

**Abstract** Understanding the structure of solid supported lipid multilayers is crucial to their application as a platform for novel materials. Conventionally, they are prepared from drop casting or spin coating of lipids dissolved in organic solvents, and lipid multilayers prepared from aqueous media and their structural characterisation have not been previously reported, due to extremely low lipid solubility (i.e.  $\sim 10^{-9}$  M) in water. Here, using X-ray reflectivity (XRR) facilitated by a “bending mica” method, we have studied the structural characteristics of dioleoylphosphatidylcholine (DOPC) multilayers prepared via drop casting aqueous small unilamellar and multilamellar vesicle or liposome (i.e. SUV and MLV) dispersions on different surfaces, including mica, positively charged polyethylenimine (PEI) coated mica, and stearic trimethylammonium iodide (STAI) coated mica which exposes a monolayer of hydrocarbon tails. We suggest that DOPC liposomes served both as a delivery matrix where an appreciable lipid concentration in water ( $\sim 25$  mg mL<sup>-1</sup> or 14 mM) was feasible, and as a structural precursor where the lamellar structure was readily retained on rupture of the vesicles at the solid surface upon solvent evaporation to facilitate rapid multilayer formation. We find that multilayers on mica from MLVs exhibited polymorphism, whereas the SUV multilayers were well ordered and showed stronger stability against water. The influence of the substrate chemistry (i.e. polymer coating, charge and hydrophobicity) on the multilayer structure is discussed in terms of lipid-substrate molecular interactions determining the bilayer packing proximal to the solid-liquid interface, which then had a templating effect on the structure of the bilayers distal from the interface, resulting in the overall different multilayer structural characteristics on different substrates. Such fundamental understanding of the correlation between the physical parameters that characterise liposomes and substrate chemistry, and the structure of lipid multilayers, underpins potential development of a simple method via an aqueous liposome dispersion route for inclusion of hydrophilic functional additives (e.g. drugs or nanoparticles) into lipid multilayer based hybrid materials, where tailored structural characteristics are an important consideration.

### 1 Introduction

Lipid bilayers have been widely studied since Mueller's description of the classic black lipid membrane (BLM) in 1960s<sup>1</sup> and Tamm and McConnell's report on supported lipid bilayers (SLBs) in 1980s<sup>2</sup>. Using SLBs as model membranes<sup>3</sup>, biological processes at the cellular level, such as viral attack<sup>4, 5</sup>, cellular signalling events<sup>6, 7</sup> and ligand-receptor interactions<sup>8-11</sup> have been investigated. In addition, SLBs have found themselves in many applications, e.g. microcontact printing<sup>12, 13</sup> and photolithography<sup>14</sup> to produce biofunctional

nanomaterials such as label free biosensors, and several reviews exist on these topics<sup>15-17</sup>.

Using lipid bilayers as building units, lipid multilayers have also been prepared in which tens to thousands of bilayers can be stacked forming ordered structures. Phosphatidylcholine lipids have been widely used, as they are the main component of cell membranes. Various applications using lipid multilayers have been developed mainly in biology<sup>18-20</sup> and nanotechnology<sup>21, 22</sup>, as model membranes to study interactions with drugs and nanoparticles, and also as a platform for functional materials. For example, dioleoylphosphatidylcholine (DOPC) lipid multilayers with thickness between 5–100 nm on silicon wafers, glass, evaporated metal films, polystyrene<sup>22</sup> and polymethyl methacrylate (PMMA)<sup>21</sup> substrates have been prepared by dip-pen nanolithography as photonic components. Similarly, DOPC, dioleoylphosphatidylethanolamine (DOPE), and dipalmitoylphosphatidylcholine (DPPC) gratings have been prepared on polydimethylsiloxane (PDMS) and glass, as potential biosensors for detection of lipid-

<sup>a</sup> School of Chemistry, University of Bristol, Cantock's Close, Bristol BS8 1TS, UK.

<sup>b</sup> XMas, The UK-CRG Beamline, The European Synchrotron (ESRF), 71 Avenue des Martyrs, 38043 Grenoble, France.

<sup>c</sup> Department of Physics, University of Warwick, Gibbet Hill Road, Coventry CV4 7AL, UK.

<sup>d</sup> Diamond Light Source, Diamond House, Harwell Science and Innovation Campus, Didcot, Oxfordshire, OX11 0DE, UK.

<sup>e</sup> Material and Interfaces Department, Weizmann Institute of Science, 76100 Rehovot, Israel.

† Email: wuge.briscoe@bristol.ac.uk; Ph: +44 (0)117 3318256.

Electronic Supplementary Information (ESI) available: [details of any supplementary information available should be included here]. See DOI: 10.1039/x0xx00000x

1 protein and lipid-drug interactions, and as a starting  
2 point for microarray development<sup>18-20</sup>. Lipid multilayers  
3 incorporating cholesterol- or sphingomyelin-enriched  
4 lipid multilayers on silica substrates have also been  
5 prepared for potential application in novel membrane-  
6 based functional materials and devices<sup>23</sup>.

7 Many studies have thus aimed to optimise lipid  
8 multilayer formation for enhanced structural order and  
9 stability. Whilst the most common method to prepare  
10 SLBs is to rupture liposomes onto a substrate, the  
11 preparation of lipid multilayers on solid surfaces involves  
12 drop casting<sup>24-30</sup> or spin coating<sup>31, 32</sup> from an organic  
13 solution of dissolved lipids (forming samples typically  
14 with thousands or tens of bilayers, respectively for the  
15 drop- and spin-casting methods). In a series of studies,  
16 Salditt *et al.*<sup>25, 28, 29, 31-35</sup> reported the formation of lipid  
17 multilayers by spin coating a lipid solution in an organic  
18 solvent onto silicon and glass substrates, showing that  
19 the number of stacked bilayers could be controlled by  
20 the volume and concentration of the solution and the  
21 spin speed. Dimyristoylphosphatidylcholine (DMPC)  
22 multilayers on silica were investigated by (X-ray  
23 reflectivity) XRR<sup>31</sup>, neutron reflectivity (NR)<sup>32, 34</sup>, atomic  
24 force microscopy (AFM), and optical microscopy<sup>32</sup>. XRR  
25 and NR profiles collected at temperature above the lipid  
26 melting temperature,  $T_m$ , revealed single crystalline  
27 membranes with the stacking of at least 10 bilayers ~5  
28 nm in thickness. This correlated well with the step size of  
29 surface features revealed by AFM imaging. However, no  
30 features were observed with optical microscopy.

31 Tristan-Nagle<sup>36</sup> reported a “rock and roll” method to  
32 prepare multilayers, in which a lipid solvent solution was  
33 deposited on the substrate fixed on a vial that was  
34 rocked and rolled manually under controlled conditions.  
35 Different substrates (*i.e.* glass, mica, and silicon wafer)  
36 and lipids (*i.e.* phosphatidylcholine (PC),  
37 phosphatidylserine (PS) and phosphatidylethanolamine  
38 (PE) with different chain lengths) were investigated. AFM  
39 imaging suggested that the multilayers were more  
40 ordered than those obtained by spin coating. Similarly to  
41 the drop casting method, the “rock and roll” method  
42 produced multilayers comprising hundreds to thousands  
43 of bilayers.

44 A main drawback for lipid multilayers is their low  
45 stability, as they are unstable in water-vapour  
46 atmosphere<sup>32</sup>, and can delaminate underwater thus  
47 losing their structural order<sup>37</sup>. Hydration of thick DOPC  
48 and dioleoyltrimethylammoniumpropane (DOTAP)  
49 multilayers (~1200 bilayers) prepared by drop casting on  
50 silicon wafer was found to lead to an increase of the  
51 lamellar spacing,  $d$ , as observed by electron density X-ray  
52 diffraction (EDXD)<sup>24</sup>. Similar results were observed by  
53 Cavalcanti *et al.*<sup>26</sup>, when anticancer drugs were  
54 intercalated in lipid multilayers formed by DPPC and

55 DOTAP. Multilayer unbinding can also be caused by  
56 heating<sup>29</sup> or by applying an electric field<sup>25</sup> to the lipid  
57 multilayer.

58 So far, all the lipid multilayer studies discussed have  
59 used organic solvents as the medium, as lipids dissolve in  
60 them readily at high concentrations (*e.g.* with  
61 concentrations of 2–20 mg mL<sup>-1</sup> typically used), and the  
62 solvent can be easily evaporated after deposition.  
63 Dissolving a mixture of different lipids in an organic  
64 solvent also affords the possibility for the formation of  
65 mixed lipid multilayers<sup>27</sup>. It would be desirable, however,  
66 to develop an alternative route from an aqueous lipid  
67 dispersion, *e.g.* to facilitate a pathway for inclusion of  
68 hydrophilic additives. However, lipid solubility in water is  
69 extremely low (with the solubility of biological lipids in  
70 the order of ~nM), making the use of water as a solvent  
71 less straightforward, with very few related studies in the  
72 literature.

73 In the present work, DOPC lipid multilayers have  
74 been prepared by drop casting an aqueous liposome  
75 dispersion on different surfaces: negatively charged  
76 mica, positively charged PEI-coated mica, and STAI-  
77 coated mica, which exposes a monolayer of hydrocarbon  
78 tails making it more hydrophobic. Use of DOPC  
79 liposomes afforded an appreciable concentration of the  
80 lipid dispersion in water (~25 mg mL<sup>-1</sup>), and also served  
81 as a structural precursor for subsequent multilayer  
82 formation during droplet evaporation. XRR was used to  
83 characterise the structure of the lipid multilayers,  
84 facilitated by a “bending mica” method<sup>38, 39, 40</sup>. Such XRR  
85 results on mica are unprecedented (and we note that  
86 neutron reflectivity has also been recently successfully  
87 applied to the mica surface<sup>41</sup>). The structures of  
88 multilayers obtained from dispersions of small  
89 unilamellar vesicles (SUVs) and multilamellar vesicles  
90 (MLVs) with different liposome sizes were compared.  
91 Polymorphism was observed in some samples, indicating  
92 the coexistence of bilayer domains with different  $d$ -  
93 spacing. The influence of different substrate chemistry  
94 on the multilayer structure is discussed in terms of lipid-  
95 substrate molecular interactions affecting the bilayer  
96 packing at the interface. Our results on the structural  
97 characteristics of the DOPC multilayers via drop casting  
98 an aqueous liposome dispersion, and their correlation  
99 with the physical parameters that characterise liposomes  
100 and substrate chemistry, are of fundamental relevance  
101 and also offer a potential route to facilitate incorporation  
102 of hydrophilic actives (*e.g.* drugs and nanoparticles) in  
103 lipid multilayer based hybrid materials.

## 104 2. Materials and Methods

### 105 2.1. Materials and sample preparation

1 DOPC lipid (>99% purity, MW = 786.113 g  
2 mol<sup>-1</sup>) in chloroform (25 mg mL<sup>-1</sup>) was  
3 purchased from Avanti® Polar Lipids,  
4 Alabaster, Alabama, and  
5 poly(ethyleneimine) (PEI; formula  
6 (CH<sub>2</sub>CH<sub>2</sub>NH)<sub>x</sub>, MW = 13,000 g mol<sup>-1</sup>) from  
7 Polymer Source™, Quebec, Canada, both  
8 used with no further purification. Its main  
9 solid-ordered (SO) to liquid-disordered  
10 (LD) transition temperature is  $T_m = -17$  °C,  
11 so that the lipid was in its LD phase at the  
12 temperature of the experiments.  
13 Surfactant stearic trimethylammonium  
14 iodide (STAI), known also as  
15 octadecyltrimethylammonium iodide  
16 (formula CH<sub>3</sub>(CH<sub>2</sub>)<sub>17</sub>N<sup>+</sup>(CH<sub>3</sub>)<sub>3</sub>I<sup>-</sup>), was  
17 prepared from  
18 octadecyltrimethylammonium chloride  
19 (STAC) as described in Ref. <sup>42</sup> and also outlined in the  
20 Electronic Supplementary Information (ESI) section.  
21 Natural muscovite mica (KAl<sub>2</sub>(Si<sub>3</sub>Al)O<sub>10</sub>(OH)<sub>2</sub>) of A1  
22 special grade was purchased from SJ Trading®, New York.  
23 Ultrapure Milli-Q® water with resistivity of 18.2 MΩ cm<sup>-1</sup>  
24 and a total organic content (ToC) of 3-4 ppb at 25 °C,  
25 chloroform (VWR, (≥99.8% purity) and nitrogen (Air  
26 Liquide, oxygen free) were used for sample preparation  
27 and XRR measurements.

28 Mica surfaces were prepared, first by cutting an  
29 original sheet (of size ~25 cm × 15 cm × 1 mm) with a  
30 pair of precision scissors, and then by hand-cleaving, into  
31 smaller pieces. They were further cut into pieces of 3 × 1  
32 cm in size and ~300 μm in thickness, as required for the  
33 XRR liquid cell<sup>39, 43</sup>. STAI coated mica (*cf.* ESI) was  
34 prepared by immersing a freshly cleaved mica piece into  
35 a 1 mg mL<sup>-1</sup> aqueous STAI solution at 70 °C for 30 s, and  
36 this was followed by immersion in Milli-Q water at 70 °C  
37 for 30 s. The contact angle of a water droplet on such  
38 STAI-coated mica was ~71° (ESI), indicating that it was  
39 more hydrophobic than bare mica. PEI-coated mica was  
40 prepared by dipping a freshly cleaved mica piece into a  
41 100 ppm polymer solution for 10 min at room  
42 temperature (RT). The STAI- and PEI-coated surfaces  
43 were then left to dry in a laminar flow hood overnight,  
44 and all the surfaces were then kept in sealed glass vials  
45 to avoid any contamination, with the mica pieces  
46 positioned in such a way that only their bottom edge and  
47 top corners came into contact with the glass vial.

## 48 2.2. Preparation of lipid multilayers

49 A designated amount of DOPC in CHCl<sub>3</sub> (25 mg mL<sup>-1</sup>) was  
50 weighed into a 7 mL glass vial, and the solvent was  
51 removed with a gentle N<sub>2</sub> stream to obtain a dried  
52 uniform crystal-free lipid film. The lipid film was first  
53 hydrated with Milli-Q water to a concentration of 14 mM  
54 and sonicated for ½ hour (h) at RT (above the DOPC  
55 melting temperature ( $T_m$ ) of -17 °C). The obtained  
56 dispersion was gently shaken manually and then the size

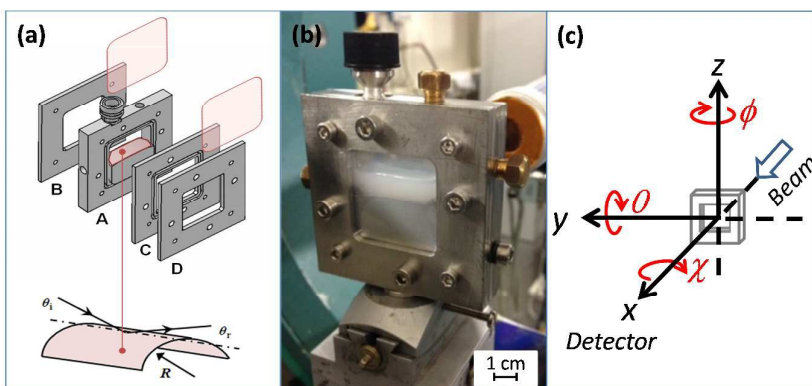


Figure 1: (a) Schematic representation of the main components of the XRR liquid cell, consisting of four stainless steel plates (A-D) and a cylindrical stage on which a 3 × 1 cm mica is gently bent. XRR measurements are made along the rigidified bending axis. (b) A photograph of the XRR liquid cell as mounted on the goniometer at ESRF beamline BM28. The white/yellow scale bar in (b) is 1 cm. (c) translational ( $x$ ,  $y$ , and  $z$ ) and rotational ( $\theta$ ,  $\phi$ , and  $\chi$ ) axis of the Huber diffractometer with respect to the XRR cell (grey, schematic), beam, and detector. (*cf.* ESI for details)

57 of the resultant liposomes was checked with dynamic  
58 light scattering (DLS), using a Malvern Nano Zetasiser ZS  
59 (Malvern Instruments, Malvern, Worcestershire, UK).  
60 DLS measurements revealed that a multilamellar vesicle  
61 (MLV) dispersion was obtained, containing a mixture of  
62 MLVs of ~150 nm in diameter, and bigger aggregates  
63 typically of size ~300-1500 nm, with a polydispersity  
64 index (PDI) ~1. These results are consistent with previous  
65 reports<sup>44, 45</sup>.

66 The MLV dispersion was then extruded through first  
67 0.4 μm and then 0.1 μm pore size polycarbonate  
68 membranes (Avanti® Polar Lipids Inc., Alabaster,  
69 Alabama) 3 times each using a LIPEX™ 10 mL  
70 Thermobarrel Extruder (Northern Lipids Inc., Burnaby,  
71 Canada) under ~20 bar pressure of N<sub>2</sub> or 21 times each  
72 using a manual Avanti® Mini Extruder apparatus (Avanti®  
73 Polar Lipids Inc., Alabaster, Alabama). DLS measurements  
74 of the obtained dispersion showed that single lamellar  
75 vesicles or liposomes (SUVs) of diameter ~90 nm with a  
76 narrow size distribution (PDI = 0.05) were formed. For  
77 drop casting, both the SUV and MLV DOPC dispersions  
78 were diluted to 2 mg mL<sup>-1</sup> with Milli-Q water, and 100 μL  
79 of each dispersion was dropped onto the substrate, with  
80 care taken to ensure that the droplet formed did not spill  
81 over the mica sheet. The samples were left to dry in a  
82 vacuum oven at RT for 2 h to ensure the removal of  
83 water, with a dried footprint of the thin film ~1 cm<sup>2</sup> in  
84 area and ~2 μm in thickness. The multilayers thus formed  
85 were kept in clean sealed vials at 4 °C until synchrotron  
86 X-ray reflectivity measurements were performed.

## 87 2.3. X-ray reflectivity (XRR) liquid cell and Synchrotron 88 XRR measurements

89 The liquid cell used in the XRR measurements (Figure 1)  
90 employs a “bending mica” method<sup>40</sup>, with a mica piece  
91 gently bent over an underlying cylindrical sample support  
92 of radius  $R = 7.5$  cm and clamped *via* two small plates.  
93 This enhances the rigidity of mica along the bending axis,  
94 thus providing sufficient flatness for the XRR

- 1 measurements along this axis. The liquid cell was
- 2 described in detail elsewhere<sup>43</sup> (see ESI for a brief
- 3 description of the liquid cell and sample alignment).

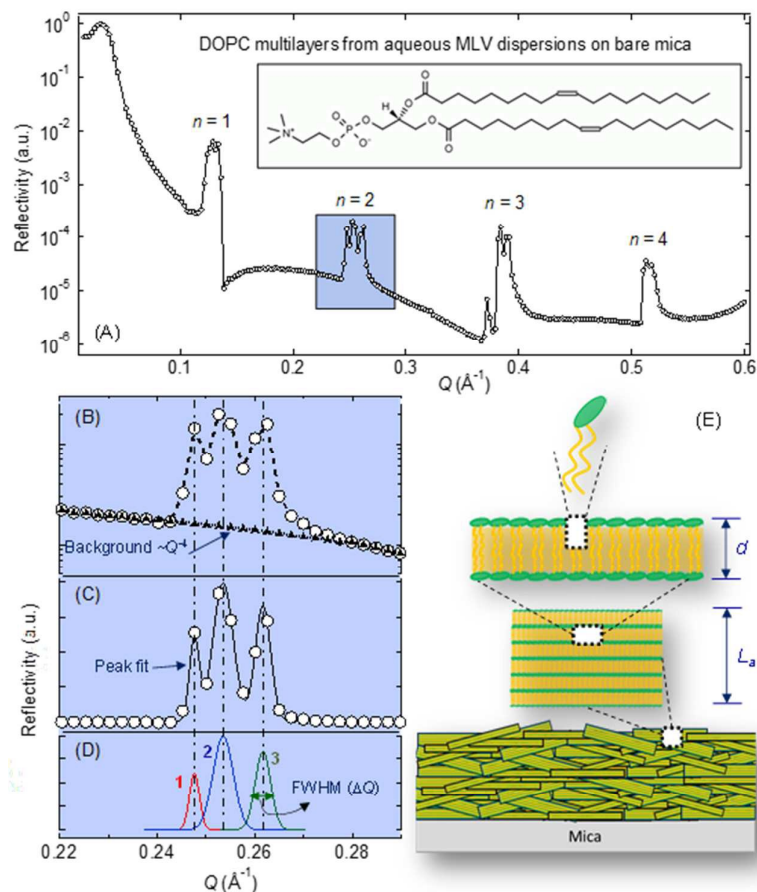


Figure 2: (A) Experimental XRR curve of DOPC multilayer from an MLV dispersion on bare mica, collected in air at room temperature. (B) An enlarged view of the reflectivity on a log-linear scale around the second order ( $n = 2$ ) Bragg peak (as enclosed in the rectangle in (A)), with the background fitted to  $Q^{-4}$ ; (C) The residual peak after background subtraction (circles), and its fit (black curve) calculated with the Igor Pro "Multipeak Fitting" operation; (D) The fitted peak could be decomposed into three Gaussian peaks (cf. Table 1), indicating polymorphism in the thin film. (E) Schematic depiction of a multilayer thin film, comprising stacked DOPC lamellar domains with the lattice plane of the bilayer (of spacing  $d$ ) approximately parallel to the substrate. The lower limit of the domain size perpendicular to the lattice plane is indicated by the coherence length ( $L_c$ ), obtained from analysis of the broadening (as defined by the FWHM  $\Delta Q$ ) of the peaks in (D) using the Scherrer equation.

24 Figure 2A shows an example XRR curve from a thin film  
 25 sample drop cast from a DOPC MLV dispersion on bare  
 26 mica. A distinct feature in the XRR curves for the DOPC  
 27 multilayer thin films in air is the presence of sharp Bragg  
 28 peaks up to the 4<sup>th</sup> order ( $n = 4$ ) of diffraction (also Figure  
 29 3A for an SUV sample), as compared to that of a bare  
 30 mica (cf. Figure 5F). These peaks are attributed to the  
 31 diffractions from the lattice planes of the highly ordered  
 32 multilayers approximately parallel to the substrate, and  
 33 the ratio of 1:2:3... in the peak  $Q_n$  positions (of order  $n =$   
 34 1, 2, 3...) is consistent with a lamellar structure. The  $d$ -  
 35 spacing, which is the lipid bilayer thickness or the  
 36 periodic distance between the lamellar lattice spacing,  
 37 can be calculated as

$$d = \frac{2n\pi}{Q_n}, \quad (1)$$

38 yielding  $d \sim 46.8\text{--}50.6 \text{ \AA}$  ( $\pm 0.2 \text{ \AA}$ ) (Table 1; MLVs),  
 39 which is consistent with a DOPC bilayer thickness<sup>24</sup>.  
 40 The error analysis details are given in ESI. The overall  
 41 shape of the curve results from the morphological  
 42 surface characteristics (*i.e.* coverage, relaxation of  
 43 the upper layer, roughness), and a detailed structural  
 44 model incorporating these features is presented

Table 1: Peaks  $Q$  position, correspondent thickness  $d$ , and coherence length  $L_c$  for the DOPC multilayers from aqueous dispersions of MLVs. The polymorphism of MLV multilayers is evident from the presence of multiple peaks (denoted as  $Q_{n,(1-4)}$ ) in the same order ( $n$ ), and up to four  $d$ -spacing values were registered, albeit not all the constituent peaks could be resolved for the Bragg peaks due to insufficient angular resolution. Errors from the fittings are reported when they are greater than 0.5% for the  $Q$  values and greater than 0.1  $\text{\AA}$  for the  $d$  spacing values. <sup>a</sup> Large uncertainties due to small number of fitted data points for the resolved peaks.

Parameter	DOPC Dispersion MLVs			
	Diffraction order $n$ (cf. Figure 2)			
	1	2	3	4
$Q_{n,1} (\text{\AA}^{-1})$	0.125	$0.247 \pm 0.003$	0.372	
$d (\text{\AA})$	50.1	$50.9 \pm 0.6$	$50.7 \pm 0.1$	
$L_c (\text{\AA})$	$808.9 \pm 50$	$3271.8 \pm \sim 1000^a$	$2408.6 \pm 236.1$	
$Q_{n,2} (\text{\AA}^{-1})$		0.253	0.383	0.511
$d (\text{\AA})$		49.6	49.2	49.1
$L_c (\text{\AA})$		$1258.9 \pm 33.5$	$1655.0 \pm 49.3$	$2539.0 \pm \sim 1000^a$
$Q_{n,3} (\text{\AA}^{-1})$	0.130	0.262	0.390	0.516
$d (\text{\AA})$	48.2	48.0	48.3	48.7
$L_c (\text{\AA})$	$1199.4 \pm 50$	$1676.6 \pm 49.3$	$1348.1 \pm 50.2$	$753.6 \pm 38.1$
$Q_{n,4} (\text{\AA}^{-1})$	0.135			
$d (\text{\AA})$	46.6			
$L_c (\text{\AA})$	2370.8			

4 XRR measurements were performed at beamline  
 5 BM28 at the European Synchrotron Radiation Facility  
 6 (ESRF), Grenoble, France, and also at beamline I07 at the  
 7 Diamond Light Source (DLS), Didcot, UK. XRR  
 8 measurements were typically made at room  
 9 temperature for all the samples in air, then water was  
 10 injected into the liquid cell and the measurement  
 11 repeated, with an integration time of  $\sim 1\text{--}5$  seconds at  
 12 each angle (*e.g.* in the range  $\theta = 0.06^\circ\text{--}2.6^\circ$   
 13 corresponding to a  $Q$  range of  $\sim 0.015$  to  $0.64 \text{ \AA}^{-1}$  for  $\lambda =$   
 14  $0.886 \text{ \AA}$  at BM28) at a typical step size of  $0.01^\circ$ , where  
 15 the momentum transfer vector normal to the sample  
 16 surface is  $Q = (4\pi \sin \theta) / \lambda$ . The specularly reflected  
 17 intensity was detected at each angle  $\theta_r = 2\theta$  by an  
 18 avalanche photodiode detector (APD) for at ESRF BM28,  
 19 and by a Pilatus 100K 2D detector at Diamond Light  
 20 Source I07. The resulting reflectivity curve can be plotted  
 21 as reflectivity (a.u.) versus  $Q (\text{\AA}^{-1})$ . Measurement details  
 22 and sample alignment procedures are given in ESI.

### 23 3. Results and Discussion

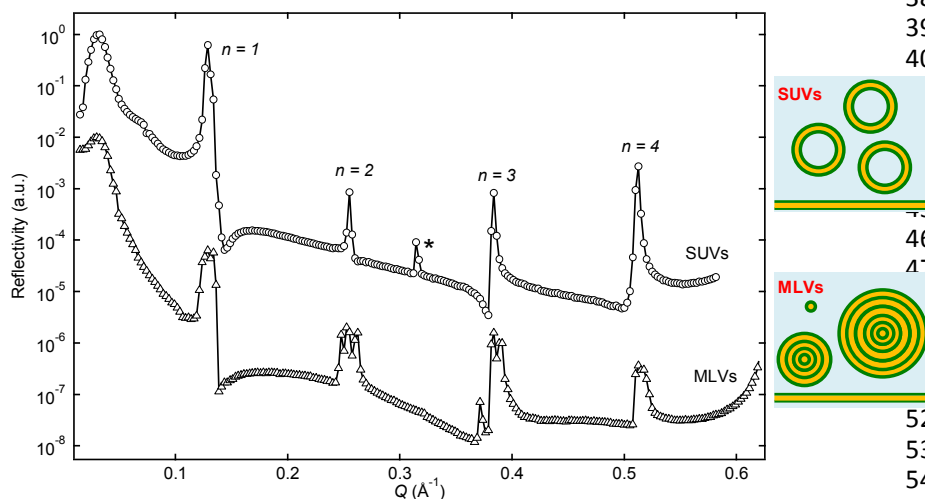


Figure 3: XRR curves for DOPC multilayers on bare mica from an SUV (circles, top curve) and an MLV (triangles, bottom curve) dispersion. The peak (marked with \*) at  $Q \sim 0.32 \text{ \AA}^{-1}$  is the mica forbidden half Bragg peak.

1 elsewhere<sup>46</sup>. At  $Q = 0.6 \text{ \AA}^{-1}$  the reflectivity from all the  
 2 samples starts to increase, a feature characteristic for  
 3 XRR curves on mica due to the presence of mica's Bragg  
 4 peak ( $Q = 0.64 \text{ \AA}^{-1}$ ). Mica's forbidden half Bragg peak ( $Q =$   
 5  $0.32 \text{ \AA}^{-1}$ ) is also present in some of the curves (always  
 6 indicated with an asterisk (\*)), which is due to mica's  
 7 monoclinic unit cell encompassing two lattice layers.

8 Within a small  $Q$  range around the Bragg peaks,  
 9 multiple peaks could be resolved, particularly  
 10 pronounced for the  $n = 2, 3$  peaks, revealing a complex  
 11 structure of the sample. Here we focus on the analysis of  
 12 the Bragg peaks using the Scherrer equation to yield the  
 13 coherence length  $L_a$ , the physical meaning for which is  
 14 the lower limit of the crystalline domain size  
 15 perpendicular to the mica surface; it thus can be used as  
 16 an indication of the structural order of the multilayer<sup>47</sup>,  
 17 <sup>48</sup>. The analysis was performed in IGOR Pro as follows. As  
 18 an example, for the 2<sup>nd</sup> order peak ( $n = 2$ ) in Figure 2A,  
 19 the reflectivity data in the  $Q$  range ( $0.22\text{--}0.29 \text{ \AA}^{-1}$ )  
 20 enclosing the peak was selected and the background  
 21 reflectivity was fitted to a 4<sup>th</sup> order polynomial (*i.e.*  $\sim Q^4$ ;  
 22 dotted black curve in Figure 2B), and subtracted from the  
 23 reflectivity data. The residual peak (circles in Figure 2C)  
 24 was subsequently fitted with the IGOR Pro "Multipeak  
 25 Fitting" operation (black curve in Figure 2C), which could  
 26 be decomposed into three Gaussian profiles (Figure 2D).  
 27 As listed in Table 1, the peak  $Q$  positions for the three  
 28 peaks (denoted as  $Q_{n,(1-3)}$  for MLVs ( $n = 2$ );  $Q_{2,1} = 0.247 \text{ \AA}^{-1}$ ,  
 29  $Q_{2,2} = 0.253 \text{ \AA}^{-1}$ , and  $Q_{2,3} = 0.262 \text{ \AA}^{-1}$ ) correspond to  
 30 three  $d$ -spacing values ( $50.9 (\pm 0.6)$ ,  $49.6$  and  $48.0 \text{ \AA}$   
 31 respectively; for the last two  $d$  values the error from the  
 32 fitting is less than  $0.01 \text{ \AA}$ ). Up to four  $d$  values were  
 33 observed due to polymorphism, although not all the  
 34 corresponding peaks could be resolved at each Bragg  
 35 peak (*cf.* Table 1). At small  $Q$  the peaks overlap more,  
 36 making it more difficult to resolve them. On the other  
 37 hand, at very high  $Q$  the reflectivity is considerably

38 diminished (as it scales  $\sim Q^{-4}$ ),  
 39 and this again could limit the  
 40 resolution in de-convoluting the  
 multiple peaks. Such a difference  
 in  $d$  could be due to different  
 lipid packing, arising from when  
 the MLVs and other lipid  
 aggregates ruptured to form  
 multilayers. It could also be due  
 46 to a slightly different residual  
 47 water content in different  
 domains, as the  $d$ -spacing of a  
 DOPC multilayer has been  
 observed to vary with the  
 variation of humidity<sup>49</sup>.

52 The full width half maximum  
 53 (Figure 2 (D)); FWHM,  $\Delta Q$ ) values  
 54 were also obtained from the  
 55 analysis. The crystalline domain  
 size (or coherent length,  $L_a$ , listed

58 in Table 1) along the direction normal to the surface is  
 59 inversely proportional to  $\Delta Q$  and can be calculated using  
 60 Scherrer's equation:<sup>50</sup>

$$61 \quad L_a = \frac{2\pi K}{\Delta Q}, \quad (2)$$

62 where  $K$  is the Scherrer constant, a shape factor  $\sim 1$  (*e.g.*  
 63 a common value is 0.94 for a cubic symmetry but it  
 64 varies depending on the shape of the crystal and on how  
 65 the width is determined). Then the number of bilayers  $m$   
 66 in the domain could be estimated as  $m = L_a/d$ .

67 In Figure 3, XRR curves of the multilayers on mica  
 68 obtained from drop casting of SUV and MLV dispersions  
 69 are compared. In contrast to the MLV sample above, the  
 70 Bragg peaks from the SUV sample are well defined single  
 71 peaks, indicating that the multilayers were largely  
 72 monomorphic with a constant  $d$  of  $49.1 \text{ \AA}$ . The  $d$  values

Table 2: The bilayer thickness  $d$ , peak position  $Q_n$ , coherence length  $L_a$ , and the corresponding number of layer in the domain ( $m$ ) for DOPC multilayers obtained from SUVs bare mica in air. Errors for  $d$  and  $Q_n$  are  $< 0.05 \%$  from the fitting.

DOPC Dispersion	SUVs				
	Diffraction Order $n$	$Q_n (\text{\AA}^{-1})$	$d (\text{\AA})$	$L_a (\text{\AA})$	No. layers $m$
	1	0.128	49.1	$1638.6 \pm 31.8$	34
	2	0.255	49.3	$2308.3 \pm 26.4$	47
	3	0.384	49.1	$2107.6 \pm 33.0$	43
	4	0.512	49.1	$1935.3 \pm 17.6$	39

Table 3: The bilayer thickness  $d$ , coherence length  $L_a$ , and the corresponding number of layer in the domain  $m$  for DOPC multilayers obtained from SUVs and MLVs on bare mica, in air and in water. Errors for  $d$  are  $< 0.1 \%$  from the fitting. a. Average values: for SUVs from all diffraction orders; for MLVs from the 2nd and 3rd resolved peaks in all diffraction orders (where present in air).

Condition	DOPC liposome dispersion	$d (\text{\AA})$	$L_a (\text{\AA})^a$	No. layers $m$
In air	SUVs	49.1	$1997.4 \pm 27.2$	41
	MLVs	49.0	$1435.8 \pm 52.2$	31
		48.3	$1291.6 \pm 62.5$	26
Under water	SUVs	62.6	$1078.3 \pm 44.1$	17
	MLVs	No Bragg peaks observed		

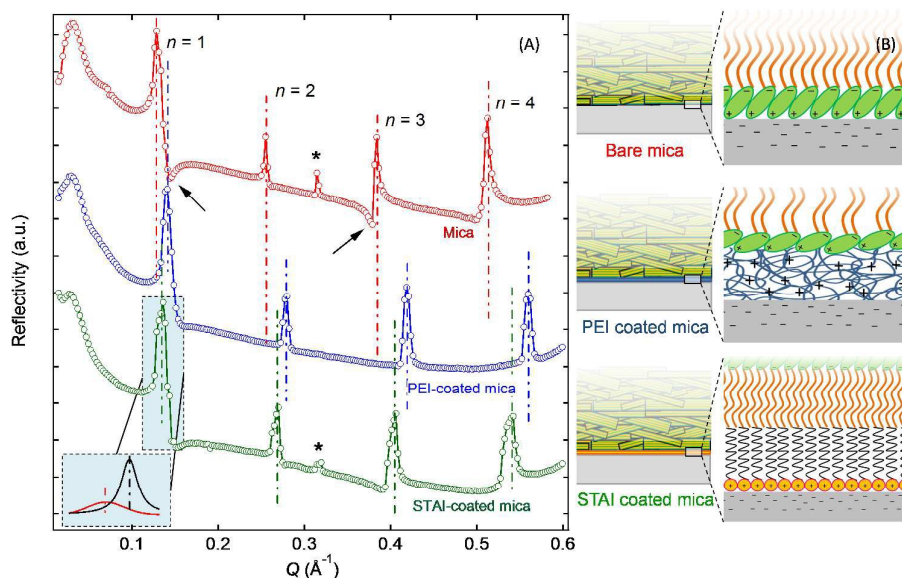


Figure 4: (A) XRR curves for DOPC on bare mica, PEI-coated mica, and STAI coated mica collected in air at room temperature. The forbidden mica half Bragg peaks are indicated by \*. The arrows indicate the presence of negative peaks, attributed to the relaxation of the top lipid layer at the air-film interface. The light blue rectangle shows a magnification of the fitting of the first Bragg peaks for the STAI-coated mica sample. (B) Schematic representation showing the three different substrates.

1 calculated from all the four orders of the Bragg peaks (*cf.*  
 2 Table 2) are also in close agreement (the errors  
 3 associated with  $d$  from each peak are smaller than 0.01  
 4 Å, and the average deviation from the mean value is 0.1  
 5 Å), further indicating well defined bilayer structures in  
 6 the multilayer lamellae. In Table 3, the DOPC multilayer  
 7 characteristics obtained for SUVs and MLVs samples are  
 8 compared. The average domain size for the SUV sample  
 9 in air ( $L_a = 1997.4 \pm 27.2$  Å) is much greater than that of  
 10 the MLV sample ( $L_a = 1339.7 \pm 59.0$  Å, calculated as the  
 11 average of the third peak of each diffraction order), and  
 12 since the lattice spacing for the two samples is almost  
 13 the same, it confirms a more ordered structure in the  
 14 case of SUVs, the number of bilayers in the domain being  
 15  $\sim 41$  for SUVs while only  $\sim 26$  for MLVs. It is conceivable  
 16 that monodispersed SUVs provided a more uniform  
 17 structural template upon rupture, leading to a more  
 18 organised structure; whereas the MLV dispersion  
 19 consisted of a plethora of aggregates in the size range  
 20  $\sim 150$ – $1500$  nm, as revealed by DLS, which frustrated  
 21 packing upon rupture at the interface, leading to both  
 22 the polymorphic and less ordered structure observed.

23 Figure 4(A) indicates that drop cast DOPC multilayers  
 24 formed on all the substrates. In the case of PEI-coated  
 25 mica, the Bragg peaks are slightly broadened ( $L_a = 1323.4$   
 26  $\pm 22.1$  Å) compared to that of the bare mica sample ( $L_a =$   
 27  $1997.4 \pm 27.2$  Å), suggesting a slightly less ordered  
 28 structure. The peaks are also shifted towards higher  $Q$   
 29 values, pointing to a slightly thinner bilayer (by  $\sim 3$  Å), as  
 30 compared to the multilayers on bare mica. All the  
 31 samples were measured under the same ambient  
 32 conditions, so it is unlikely that the structural differences  
 33 were due to different relative humidity, and  
 34 consequently different hydration, levels. PEI and mica

35 would have exhibited different surface charge densities,  
 36 and the interfacial roughness on PEI-coated mica is  
 37 expected to be slightly higher. We thus attribute the  
 38 observed structural differences to the interactions  
 39 between the DOPC headgroups and the PEI layer. The  
 40 dipole of the zwitterionic headgroup is oriented with the  
 41 negative charge proximal, and the positive charge distal,  
 42 to the tail. The outermost positive charge enables PC-  
 43 lipids to attach to mica and to negatively charged  
 44 polymers. In the case of the positively charged PEI-  
 45 coated mica, the headgroups must adopt an orientation  
 46 and arrangement different from that on bare mica  
 47 (schematically shown in Figure 4(B)), and this would  
 48 consequently result in different lipid packing in the  
 49 bilayer immediately adjacent to the surface. A thinner  
 50 bilayer suggests that either tilting or interdigitation of  
 51 the lipid tails occurred<sup>39</sup>, due to a slightly relaxed  
 52 packing. It is curious and interesting that the Bragg peaks  
 53 from the PEI-coated mica sample are monomorphic,  
 54 which indicates that the surface bilayer had a templating  
 55 effect and the bilayer packing was largely retained  
 56 throughout the thin film.

57 In the case of more hydrophobic STAI-coated mica as  
 58 the substrate, the DOPC multilayer thin film exhibited  
 59 polymorphism, for instance with the two decomposed  
 60 peaks from the  $n = 1$  Bragg peak shown in the inset at  
 61 the bottom left corner of Figure 4, with corresponding  $d$ -  
 62 spacing and coherence length values of ( $d = 47.8$  Å,  $L_a =$   
 63  $747.1$  Å) and ( $d = 46.1$  Å,  $L_a = 1603.6$  Å) respectively (the  
 64 errors in the thicknesses  $d$ , and full width at half  
 65 maximum  $\Delta Q$ , from the fitting is  $\sim 0$  Å, thus the error on  
 66  $L_a$  is also almost null). That is, the film constituted  
 67 domains with (at least) two different lattice spacing, and  
 68 those with slightly thinner bilayers were more ordered. It

1 is conceivable that, upon encountering the hydrophobic  
2 STAI monolayer, the DOPC SUVs would rupture and also  
3 need to undergo cleavage so that the hydrophobic lipid  
4 tails are unzipped from the liposome bilayers, facing  
5 towards and in intimate contact with the STAI layer. The  
6 packing density of the tails would be influenced by that  
7 of the STAI monolayer and also the STAI surface  
8 coverage. Subsequent surface templating effects would  
9 lead to such bilayer structures being largely retained  
10 throughout the film.

11 A noticeable feature in the XRR curves of the SUV  
12 DOPC multilayer thin film on bare mica is the “negative”  
13 peaks, as indicated by two arrows in Figure 4. As a  
14 detailed structural model shows,<sup>51</sup> this is due to the  
15 relaxation of the terminating monolayer at the air-film  
16 interface, most pronounced on bare mica and much less  
17 so on more hydrophobic STAI-coated mica and absent on  
18 PEI-coated mica.



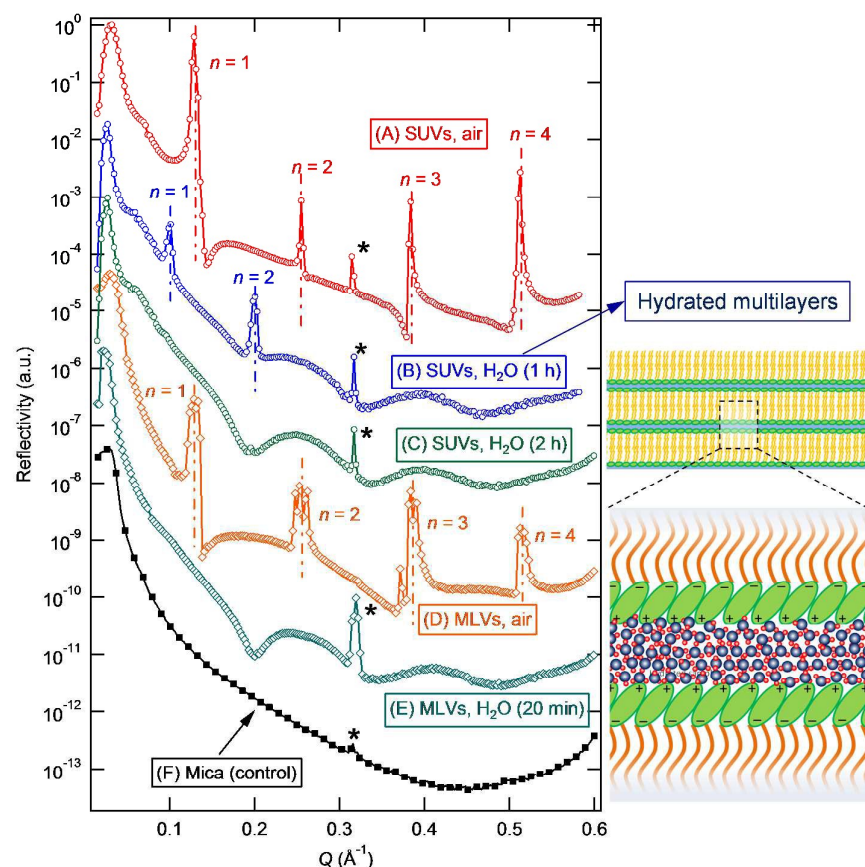


Figure 5: XRR curves of SUV DOPC multilayers on mica in air (A), in water after 1 h (B) and 2 h immersion (C). XRR curves of MLV DOPC multilayers on mica in air (D), and in water after 20 min immersion (E). For comparison, the XRR curve of a control bare mica piece in air (*i.e.* without any DOPC layers) is shown in (F). The hydrated multilayers in the SUV sample under water (Curve B) are shown schematically on the right hand side, with a hydration layer of thickness  $\Delta d \sim 13.5 \text{ \AA}$  per bilayer, corresponding to 4-5 molecular water layers.

1 It is known that lipid membranes are not stable under  
 2 water<sup>52</sup> and bilayers tend to delaminate from lipid  
 3 membranes<sup>32, 37</sup>. It is important to understand the  
 4 structural transition of lipid multilayers under water, a  
 5 rapid process difficult to probe experimentally. Relatively  
 6 fast XRR scans due to the high synchrotron X-ray flux  
 7 have allowed us to compare the XRR curves of the DOPC  
 8 multilayers from SUVs and MLVs at the initial stage of  
 9 water submersion (Figure 5). After 1 h under water, the  
 10 Bragg peaks from the SUV DOPC multilayers shifted  
 11 towards lower  $Q$  (Figure 5B), consistent with thicker  
 12 bilayers ( $d = 62.6 \text{ \AA}$ ) due to hydration of the headgroups.  
 13 As compared to  $d = 49.1 \text{ \AA}$  in the ambient air, this  
 14 represents bilayer swelling of  $\Delta d \sim 13.5 \text{ \AA}$ , corresponding  
 15 to a hydration layer with 4-5 molecular water layers per  
 16 bilayer. Similar swelling behaviour due to hydration has  
 17 also been previously observed for supported purple  
 18 membranes<sup>53, 54</sup> using XRR. Furthermore, the Bragg  
 19 peaks of hydrated samples are broader and less intense  
 20 than those of dry multilayers, with an  $L_a = 1078.3 \pm 44.1$   
 21  $\text{\AA}$  as compared to  $L_a = 1997.4 \pm 27.2 \text{ \AA}$  in air (*cf.* Table 3),  
 22 and the 3<sup>rd</sup> and 4<sup>th</sup> Bragg peaks are also absent. The loss  
 23 of crystalline long-range order is due to lattice defects

24 and bending fluctuations in  
 25 addition to water-induced  
 26 bilayer undulations, which would  
 27 also give rise to variations in the  
 28 bilayer thickness. However, no  
 29 significant peak splitting (*i.e.*  
 30 polymorphism) was observed.  
 31 These observations suggest that  
 32 bilayer hydration occurred soon  
 33 after water addition, and the  
 34 swelling of the bilayers was  
 35 largely uniform, with water  
 36 molecules permeating through  
 37 the multilayer structure. This  
 38 resulted in swollen bilayers, with  
 39 an overall less ordered  
 40 multilayer structure. Our results  
 41 from a separate experiment  
 42 (Figure S2 in ESI) show that the  
 43 DOPC multilayer structure could  
 44 be retained up to  $\sim 2 \text{ h}$  in water,  
 45 where similar bilayer swelling  
 46 was also observed.

47 Prolonged water submersion  
 48 led to the loss of the multilayer  
 49 structure, evident from the  
 50 disappearance of the Bragg  
 51 peaks (Figure 5C; 2 h in water in  
 52 this particular experiment).  
 Instead, mild reflectivity  
 oscillations called Kiessig fringes  
 appear due to a lipid bilayer of  
 thickness  $\sim 45.3 \text{ \AA}$  remaining at  
 the mica-water interface<sup>39</sup>.

Table 4: Bilayer thickness  $d$ , coherence length  $L_a$  (from  $n = 1$  Bragg peak), and the minimum number of bilayer  $m$  in the lamellae domain for SUV DOPC multilayers on bare, PEI- and STAI-coated mica. For comparison, the  $L_a$  and  $m$  values obtained from the paracrystalline disorder analysis are also reported. Errors for  $d$  are not reported as they are almost null (*i.e.* at least  $< 0.05 \%$ ) from the fitting. <sup>a</sup>Values correspond to the two decomposed peaks (*cf.* Figure 4A). <sup>b</sup>Multiple peaks are present for each Bragg peak due to polymorphism but not all resolved at each Bragg peak; here the third peak ( $Q_{n,3}$ ) of the decomposed peaks from  $n = 1, 2, 3$ , and 4 Bragg peaks in the XRR curve for the MLV DOPC multilayer sample is used, which has also allowed the paracrystalline disorder parameter  $g$  (Figure 6) to be extracted.

Substrate for SUV DOPC multilayer	$d$ ( $\text{\AA}$ )	$L_a$ ( $\text{\AA}$ )	No. layers $m$	Paracrystalline disorder parameter $g$	$L_a$ ( $\text{\AA}$ ) from Fig.6 and Eq.(4)	No. Layers $m$
Bare mica	49.1	$1997.4 \pm 27.2$	41	$\sim 0$	NA	NA
PEI-coated mica	45.0	$1323.4 \pm 22.1$	29	$0.0177 \pm 0.0003$	$1480 \pm 77$	33
STAI-coated mica <sup>a</sup>	47.8	$747.1 \pm 10$	16	NA	NA	NA
	46.1	$1603.6 \pm 10$	35	$0.0248 \pm 0.0004$	$1854 \pm 523$	40
MLV DOPC multilayer on bare mica <sup>b</sup>	48.3	$1259.4 \pm 41.9$	26	$0.0252 \pm 0.0003$	$1581 \pm 384$	33

1 Detailed analysis of these Kiessig fringes requires  
 2 consideration of the crystal truncation rods of mica<sup>39, 43</sup>,  
 3 and will be presented in a further publication<sup>46</sup>.

4 For the DOPC multilayers prepared from a MLV  
 5 dispersion, the Bragg peaks are absent in the XRR curve  
 6 collected 20 min after water addition (Figure 5D, E),  
 7 suggesting a less stable film as compared to the SUV  
 8 sample. Similarly, Kiessig fringes indicate the presence of  
 9 a bilayer at the mica-water interface of thickness  $d \sim 44.1$   
 10  $\text{\AA}$ <sup>46</sup>, in close agreement with that for the remnant  
 11 bilayers in the SUV sample under water ( $\sim 45.3 \text{\AA}$ ). Our  
 12 results indicate that, in addition to a more ordered  
 13 structure, the multilayers from the SUV dispersion  
 14 showed better stability against water, probably due to  
 15 fewer structural defects where delamination of the  
 16 multilayers would be initiated. We have also  
 17 subsequently incubated the sample with a DOPC SUV  
 18 dispersion; however, the multilayers were not re-formed  
 19 in the solution (*cf.* Figures S3D, E in ESI). In addition to  
 20 the finite crystalline domain size as characterised by the  
 21 coherence length  $L_a$ , the lattice spacing fluctuations (*i.e.*  
 22 the paracrystalline disorder) may also contribute to the  
 23 broadening of the Bragg peaks<sup>55</sup>, which is consequently  
 24 accompanied by a decrease in the peak intensity. This  
 25 originates from the crystallites with slightly different  $d$ -  
 26 spacing values, manifesting in increased broadening of  
 27 the Bragg peaks with increasing diffraction orders  $n$ . This  
 28 is evident from the reduced  $L_a$  values in Table 1 for  
 29 higher order peaks ( $n = 3, 4$ ) in the case SUV DOPC  
 30 multilayers on mica. This means that the Scherrer  
 31 equation is insufficient on its own to fully describe the  
 32 structural order due to bilayer thickness fluctuations in  
 33 the multilayer film, and a correction should be applied.  
 34 The two contributions from the crystallite size and the  
 35 distortion caused by the paracrystalline disorder may be  
 36 separated by plotting the broadening of each peak  
 37  $((\Delta Q)^2/(2\pi)^2)$  versus the fourth power of the diffraction  
 38 order ( $h^4$ ) for a plane of Miller index  $(h00)$ .<sup>47, 56, 57</sup> From  
 39 the linear fit to the plot,  $y = y_0 + mh^4$ , the coherence  
 40 length,  $L_a$ , and the degree of disorder in the crystal,  $g$ ,  
 41 can be inferred respectively from the intercept  $y_0$  and  
 42 the slope  $m$  as

$$43 \quad g = \frac{1}{\pi} (md^2)^{1/4}, \quad (3)$$

$$44 \quad \text{and} \quad L_a = (y_0)^{-1/2}. \quad (4)$$

45 Figure 6 shows such a plot for the SUV DOPC  
 46 multilayers in air on mica, PEI- and STAI-coated mica,  
 47 as well as the MLV multilayer sample, for which at least  
 48 three orders of reflections have been observed to allow  
 49 this plot.<sup>55</sup> For SUV multilayers on mica, the bilayer  
 50 thickness fluctuation is small and thus the slope of the  
 51 plot is null ( $m \sim 0$ ). The paracrystalline disorder  
 52 parameter  $g$  (*cf.* Table 4) for the multilayer on the STAI-  
 53 coated mica ( $0.0248 \pm 0.0003$ ) is greater than that for the  
 54 PEI-coated sample ( $0.0177 \pm 0.0007$ ), and the MLV  
 55 sample showed a degree of paracrystalline disorder ( $g =$

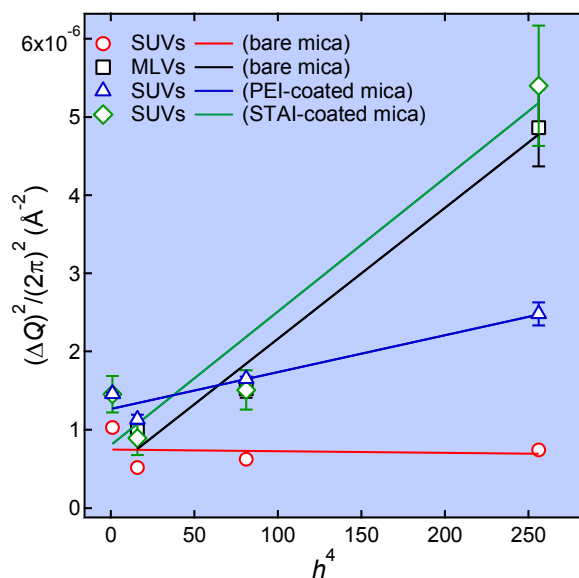


Figure 6: Peak broadening  $(\Delta Q)^2/(2\pi)^2$  of lamellar reflections as a function of the fourth power of the diffraction order  $h^4$  for DOPC multilayers from MLVs on bare mica (squares), and SUVs on bare mica (circles), on PEI-coated mica (triangles), and STAI-coated mica (diamonds). From the slopes  $m$  of the linear fits ( $y = y_0 + mx$ ), the paracrystalline disorder parameters  $g$  could be calculated from Eq. (3). From the intercept  $y_0$ , the coherence length  $L_a$  could be estimated from Eq. (4). These values are listed in Table 4. The error bars for the SUV multilayers on mica are smaller than the circles and thus invisible.

56  $0.0252 \pm 0.0003$ ) similar to that on STAI. The conclusion  
 57 on the structural order from such an analysis thus  
 58 concurs with that by the Scherrer equation analysis. The  
 59 obtained  $L_a$  values, also listed in Table 4, are comparable  
 60 to those obtained from the Scherrer equation. Overall,  
 61 the multilayers prepared from the SUV dispersions are  
 62 more ordered than those from the MLVs, with larger  
 63 crystalline domain sizes and smaller bilayer thickness  
 64 perturbations. The number of layers  $m$  calculated using  
 65 values obtained from Equations (3) and (4) are reported  
 66 in Table 4, which are slightly higher than those obtained  
 67 from the Scherrer equation, but follow the same trend.

## 68 4. Conclusions

69 In the present work, DOPC multilayers have been  
 70 prepared by drop casting aqueous dispersions of  
 71 liposomes on different substrates, and the multilayer  
 72 structure has been studied using the synchrotron XRR  
 73 technique, facilitated by a unique “bending mica”  
 74 method<sup>43</sup>. In general, ordered lamellar structures  
 75 consisting of DOPC bilayer domains have been obtained,  
 76 with the lattice planes aligned approximately parallel to  
 77 the substrate, evident from the distinct Bragg diffraction  
 78 peaks in the XRR curve. The Bragg peaks have been  
 79 analysed, using both the Scherrer equation and in terms  
 80 of the degree of paracrystalline disorder, to yield  
 81 detailed structural information. The multilayers prepared  
 82 from monodispersed, well defined small unilamellar  
 83 liposomes/vesicles (SUVs)  $\sim 90$ – $100$  nm in diameter were

1 more ordered than those from multilamellar  
2 liposomes/vesicles (MLVs). This manifested as a larger  
3 coherence length (or domain size) perpendicular to the  
4 substrate, and an almost zero paracrystalline disorder  
5 parameter, which indicates little fluctuations in the  
6 bilayer thickness throughout the thin film. The MLV  
7 multilayers showed polymorphism, with multiple Bragg  
8 peaks observed, exhibiting a number of different bilayer  
9 thicknesses.

10 The SUV multilayers also showed stronger stability  
11 against water as compared to the MLV multilayers,  
12 retaining the Bragg peaks in water for up to 2 hours. This  
13 observation again points to a more ordered structure  
14 with fewer defects in the domains, where delamination  
15 of the multilayer would be initiated. Relative fast XRR  
16 scans allowed us to study the rapid structural transition  
17 as the multilayers were submerged under water. We  
18 found that bilayers became swollen rapidly, with a  
19 hydration layer of thickness corresponding to 4-5 water  
20 molecular layers per bilayer.

21 We have also found that the surface chemistry of the  
22 substrate affected the multilayer structure. The  
23 multilayers cast on PEI- and STAI-coated mica from DOPC  
24 SUV dispersions had a higher degree of paracrystalline  
25 disorder than those on bare mica, with the STAI-coated  
26 mica, more hydrophobic compared to bare and PEI-  
27 coated mica, showing a greater effect, leading to  
28 structural polymorphism in the multilayers. This could be  
29 attributed to the interactions between the rupturing  
30 liposomes with the surface layer, dominating lipid  
31 packing immediately adjacent to the interface, which  
32 interestingly was templated by the bilayer domains  
33 subsequently formed, with the bilayer structure retained  
34 throughout the film. This highlights the importance of  
35 the substrate chemistry, and conversely offers a  
36 mechanism to tune the multilayer structure by  
37 controlling the surface charge and wettability.

38 Previously, lipid multilayers have been typically  
39 prepared from an organic solvent, due to the extremely  
40 low solubility of lipids in water. We suggest that DOPC  
41 liposomes serve a dual role. They act as a delivery matrix  
42 – here an appreciable lipid concentration in water (up to  
43  $\sim 25 \text{ mg mL}^{-1}$  or 14 mM) was feasible. In addition, they  
44 serve as a structural precursor, with their lamellar  
45 structure readily retained upon rupture at the solid  
46 surface upon evaporation to facilitate rapid multilayer  
47 formation. Pre-forming such liposomes in aqueous media  
48 would also offer a mechanism to incorporate desired  
49 functional ingredients in the lamellar structure, which  
50 could be readily transferred to the multilayers. Other  
51 potential variables such as controlling the evaporation  
52 rate *via* temperature and using solvent mixtures could  
53 offer further mechanisms for tailoring the multilayer  
54 structure and await future exploitation. Our results  
55 represent first detailed structural characterisation of  
56 lipid multilayers *via* the pathway of drop casting aqueous  
57 liposome dispersions, pointing to controlled preparation

58 of ordered lipid multilayers by tailoring the liposome  
59 homogeneity and substrate surface properties,  
60 potentially offering a simple method for inclusion of  
61 hydrophilic and hydrophobic functional additive (*e.g.*  
62 drugs or nanoparticles; Sironi *et al.*, in preparation<sup>46</sup>) in  
63 lipid multilayer based hybrid materials.

## 64 Acknowledgements

65 We would like to acknowledge funding from the  
66 Engineering and Physical Science Research Council  
67 (EPSRC), the Royal Society, the European Research  
68 Council (ERC, Advanced Grant HydrationLube, awarded  
69 to J.K.), Taiho Kogyo Tribology Research Foundation  
70 (TTRF), the European Cooperation in Science and  
71 Technology (CMST COST) Action CM1101, and the Marie  
72 Curie Initial Training Network (MC-ITN) NanoS3. We also  
73 thank the European Synchrotron Radiation Source (ESRF)  
74 and Diamond Light Source (Expt. number SI13139) for  
75 access to synchrotron X-ray sources. The XMaS-BM28  
76 beamline is a mid-range facility supported by EPSRC, and  
77 we are grateful to all the beam line team staff for their  
78 support. XRR data extraction was performed using an  
79 Igor Pro software package developed by T. Dane  
80 (presently at ESRF). A.S. and T.S. were supported by  
81 EPSRC CASE Awards, and C.R. by an Everett Scholarship.

82

## 83 Notes and references

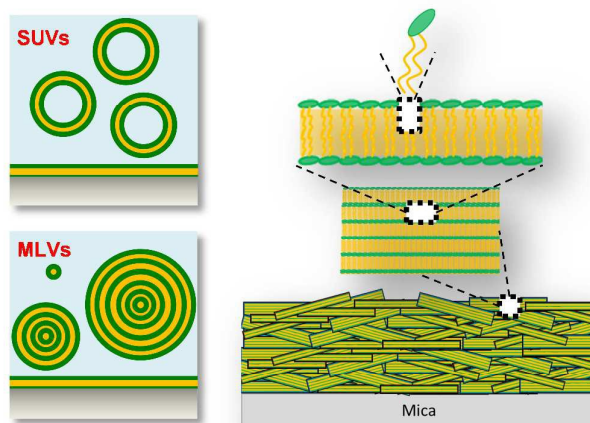
- 84 1. P. Mueller, H. T. Tien, W. C. Wescott and D. O. Rudin,  
85 *Circulation*, 1962, **26**, 1167-1171.
- 86 2. L. K. Tamm and H. M. McConnell, *Biophys J*, 1985, **47**,  
87 105-113.
- 88 3. M. Eeman and M. Deleu, *Biotechnol Agron Soc*, 2010,  
89 **14**, 719-736.
- 90 4. M. Mazzon and J. Mercer, *Cell Microbiol*, 2014, **16**,  
91 1493-1502.
- 92 5. G. Bilek, N. M. Matscheko, A. Pickl-Herk, V. U. Weiss, X.  
93 Subirats, E. Kenndler and D. Blaas, *J Virol*, 2011, **85**,  
94 8368-8375.
- 95 6. K. Simons and D. Toomre, *Nat Rev Mol Cell Biol*, 2000,  
96 **1**, 31-39.
- 97 7. J. A. Allen, R. A. Halverson-Tamboli and M. M.  
98 Rasenick, *Nat Rev Neurosci*, 2007, **8**, 128-140.
- 99 8. T. Yang, O. K. Baryshnikova, H. Mao, M. A. Holden and  
100 P. S. Cremer, *JACS*, 2003, **125**, 4779-4784.
- 101 9. H. Jung, A. D. Robison and P. S. Cremer, *J Struct Biol*,  
102 2009, **168**, 90-94.
- 103 10. M. Gavutis, S. Lata, P. Lamken, P. Müller and J. Piehler,  
104 *Biophys J*, 2005, **88**, 4289-4302.
- 105 11. S. Majd and M. Mayer, *Angew Chem*, 2005, **117**, 6855-  
106 6858.
- 107 12. A. P. Quist, E. Pavlovic and S. Oscarsson, *Anal Bioanal*  
108 *Chem*, 2005, **381**, 591-600.
- 109 13. J. Chalmeau, C. le Grimellec, J. Sternick and C. Vieu,  
110 *Colloids Surf B Biointerfaces*, 2012, **89**, 188-195.
- 111 14. C. K. Yee, M. L. Amweg and A. N. Parikh, *Adv Mater*,  
112 2004, **16**, 1184-1189.
- 113 15. J. A. Jackman, W. Knoll and N.-J. Cho, *Materials*, 2012,  
114 **5**, 2637-2657.

- 1 16. E. T. Castellana and P. S. Cremer, *Surf Sci Rep*, 2006, **61**,  
2 429-444.
- 3 17. Y. K. Lee, H. Lee and J.-M. Nam, *NPG Asia Mater*, 2013,  
4 **5**, e48.
- 5 18. A. E. Kusi-Appiah, N. Vafai, P. J. Cranfill, M. W.  
6 Davidson and S. Lenhart, *Biomaterials*, 2012, **33**, 4187-  
7 4194.
- 8 19. O. A. Nafday and S. Lenhart, *Nanotechnology*, 2011,  
9 **22**, 1-7.
- 10 20. O. A. Nafday, T. W. Lowry and S. Lenhart, *Small*, 2012,  
11 **8**, 1021-1028.
- 12 21. S. Lenhart, F. Brinkmann, T. Laue, S. Walheim, C.  
13 Vannahme, S. Klinkhammer, M. Xu, S. Sekula, T.  
14 Mappes, T. Schimmel and H. Fuchs, *Nat Nano*, 2010, **5**,  
15 275-279.
- 16 22. S. Lenhart, P. Sun, Y. Wang, H. Fuchs and C. A. Mirkin,  
17 *Small*, 2007, **3**, 71-75.
- 18 23. L. Tayebi, Y. Ma, D. Vashaee, G. Chen, S. K. Sinha and A.  
19 N. Parikh, *Nat Mater*, 2012, **11**, 1074-1080.
- 20 24. R. Caminiti, G. Caracciolo, M. Pisani and P. Bruni, *Chem*  
21 *Phys Lett*, 2005, **409**, 331-336.
- 22 25. D. Constantin, C. Ollinger, M. Vogel and T. Salditt, *Eur*  
23 *Phys J E*, 2005, **18**, 273-278.
- 24 26. L. P. Cavalcanti, H. Haas, H. N. Bordallo, O. Kononov,  
25 T. Gutberlet and G. Fragneto, *Eur Phys J Spec Top*,  
26 2007, **141**, 217-221.
- 27 27. H. Y. Jing, D. H. Hong, B. D. Kwak, D. J. Choi, K. Shin, C.  
28 J. Yu, J. W. Kim, D. Y. Noh and Y. S. Seo, *Langmuir*,  
29 2009, **25**, 4198-4202.
- 30 28. T. Salditt, C. Li, A. Spaar and U. Mennicke, *Eur Phys J E*,  
31 2002, **7**, 105-116.
- 32 29. M. Vogel, C. Münster, W. Fenzl and T. Salditt, *Phys Rev*  
33 *Lett*, 2000, **84**, 390-393.
- 34 30. M. Seul and M. J. Sammon, *Thin Solid Films*, 1990, **185**,  
35 287-305.
- 36 31. U. Mennicke and T. Salditt, *Langmuir*, 2002, **18**, 8172-  
37 8177.
- 38 32. L. Perino-Gallice, G. Fragneto, U. Mennicke, T. Salditt  
39 and F. Rieutord, *Eur Phys J E*, 2002, **8**, 275-282.
- 40 33. T. Salditt, C. Munster, J. Lu, M. Vogel, W. Fenzl and A.  
41 Souvorov, *Phys Rev E*, 1999, **60**, 7285-7289.
- 42 34. C. Munster, T. Salditt, M. Vogel, R. Siebrecht and J.  
43 Peisl, *Europhys Lett*, 1999, **46**, 486-492.
- 44 35. T. Salditt, *J Phys Condens Matter*, 2005, **17**, R287.
- 45 36. S. Tristram-Nagle, in *Methods in Membrane Lipids*, ed.  
46 A. Dopico, Humana Press, 2007, vol. 400, ch. 5, pp. 63-  
47 75.
- 48 37. A. C. Simonsen and L. A. Bagatolli, *Langmuir*, 2004, **20**,  
49 9720-9728.
- 50 38. M. C. Duff, *Am Mineral*, 2004, **89**, 254-254.
- 51 39. F. Speranza, G. A. Pilkington, T. G. Dane, P. T.  
52 Cresswell, P. Li, R. M. J. Jacobs, T. Arnold, L.  
53 Bouchenoire, R. K. Thomas and W. H. Briscoe, *Soft*  
54 *Matter*, 2013, **9**, 7028-7041.
- 55 40. W. H. Briscoe, M. Chen, I. E. Dunlop, J. Klein, J. Penfold  
56 and R. M. J. Jacobs, *J Colloid Interface Sci*, 2007, **306**,  
57 459-463.
- 58 41. K. L. Browning, L. R. Griffin, P. Gutfreund, R. D. Barker,  
59 L. A. Clifton, A. Hughes and S. M. Clarke, *J Appl*  
60 *Crystallogr*, 2014, **47**, 1638-1646.
- 61 42. G. Silbert, J. Klein and S. Perkin, *Farad Discuss*, 2010,  
62 **146**, 309-324.
- 63 43. W. H. Briscoe, F. Speranza, P. X. Li, O. Kononov, L.  
64 Bouchenoire, J. van Stam, J. Klein, R. M. J. Jacobs and  
65 R. K. Thomas, *Soft Matter*, 2012, **8**, 5055-5068.
- 66 44. M. J. Hope, M. B. Bally, L. D. Mayer, A. S. Janoff and P.  
67 R. Cullis, *Chem Phys Lipids*, 1986, **40**, 89-107.
- 68 45. A. Jesorka and O. Orwar, in *Annu Rew Anal Chem*,  
69 2008, vol. 1, pp. 801-832.
- 70 46. B. Sironi, T. Snow, C. Redeker, J. Bartenstain, O.  
71 Bikondoa, J. Klein and W. H. Briscoe, *In Prep.*
- 72 47. T. G. Dane, P. T. Cresswell, O. Bikondoa, G. E. Newby, T.  
73 Arnold, C. F. J. Faul and W. H. Briscoe, *Soft Matter*,  
74 2012, **8**, 2824-2832.
- 75 48. P. Scherrer, *Göttinger Nachrichten Gesell*, 1918, **2**, 98.
- 76 49. Y. Ma, S. K. Ghosh, S. Bera, Z. Jiang, S. Tristram-Nagle,  
77 L. B. Lurio and S. K. Sinha, *Phys Chem Chem Phys*, 2015,  
78 **17**, 3570-3576.
- 79 50. A. L. Patterson, *Phys Rev*, 1939, **56**, 978-982.
- 80 51. B. Sironi, T. Snow, J. Klein and W. H. Briscoe, *In Prep.*,  
81 2016.
- 82 52. G. Gupta, S. Iyer, K. Leasure, N. Virdone, A. M.  
83 Dattelbaum, P. B. Atanassov and G. P. López, *ACS*  
84 *Nano*, 2013, **7**, 5300-5307.
- 85 53. N. H. M. Kaus, A. M. Collins, O. Bikondoa, P. T.  
86 Cresswell, J. M. Bulpett, W. H. Briscoe and S. Mann, *J*  
87 *Mater Chem C*, 2014, **2**, 5447-5452.
- 88 54. A. M. Collins, N. H. Mohd Kaus, F. Speranza, W. H.  
89 Briscoe, D. Rhinow, N. Hampp and S. Mann, *J Mater*  
90 *Chem*, 2010, **20**, 9037-9041.
- 91 55. R. Hosemann and A. M. Hindeleh, *J Macromol Sci-Phys*,  
92 1995, **B34**, 327-356.
- 93 56. T. G. Dane, P. T. Cresswell, G. A. Pilkington, S. Lilliu, J. E.  
94 Macdonald, S. W. Prescott, O. Bikondoa, C. F. J. Faul  
95 and W. H. Briscoe, *Soft Matter*, 2013, **9**, 10501-10511.
- 96 57. S. Lilliu, T. Agostinelli, E. Pires, M. Hampton, J. Nelson  
97 and J. E. Macdonald, *Macromolecules*, 2011, **44**, 2725-  
98 2734.

## Structure of lipid multilayers *via* drop casting of aqueous liposome dispersions

*Beatrice Sironi<sup>1</sup>, Tim Snow<sup>1</sup>, Christian Redeker<sup>1</sup>, Anna Slastanova<sup>1</sup>, Oier Bikondoa<sup>2,3</sup>, Thomas Arnold<sup>4</sup>, Jacob Klein<sup>5</sup>, and Wuge H. Briscoe<sup>1\*</sup>*

Liposomes serve as a lipid delivery matrix and a structural precursor, facilitating solid-supported lipid



multilayer formation via simple drop casting.